

POROSITY AND ITS MEASUREMENT*

LAURA ESPINAL

Material Measurement Laboratory, National Institute of Standards and Technology, Gaithersburg, MD, USA

INTRODUCTION

Porosity is one of the factors that influences the physical interactions and chemical reactivity of solids with gases and liquids for many industrial applications. The examples of industrially important porous materials include catalysts, construction materials, ceramics, pharmaceutical products, pigments, sorbents, membranes, electrodes, sensors, active components in batteries and fuel cells, and oil and gas bearing strata and rocks. The volume fraction of porosity (ε) can be defined as the fraction of void space (V_v) relative to the apparent total bulk volume (V_T) of the sample (Equation 1) (Klobes et al., 2006). For a single phase material, the value of V_v can be obtained from the difference between the volume of the solid (computed from its crystal lattice density) and the apparent total bulk volume (V_T) of the sample:

$$\varepsilon = \frac{V_v}{V_T} \quad (1)$$

Porosity in materials originates from different processing and synthesis routes (Klobes et al., 2006; Rouquerol et al., 1994a). Synthesis of porous crystalline materials, such as zeolites and metal organic frameworks, leads to highly regular intracrystalline pore networks in addition to inherent voids imparted by the presence of vacancies, grain boundaries, and interparticle spaces (Auerbach et al., 2003). As a simplified measure, pore size (or width) is referred to the smallest dimension within a given pore shape, that is, the width between two opposite walls for a slit-shaped pore and the diameter for a cylindrical pore (Rouquerol et al., 1999). Some zeolite crystal structures with their characteristic pore sizes are shown in Figure 1. Porous materials can also be fabricated through the bonding of finely divided nonporous particles (e.g., sand) that form agglomerates at specific pressure and temperature conditions, which results in interparticle void space (Rahaman, 2003). Figure 2 shows a schematic of an agglomerate of polycrystalline particles containing voids in between particles (Rahaman, 2003). Another route to porous solids constitutes direct self-assembly of particles, examples of such structures can be found in references (Deng et al., 2005; Warren et al., 2008).

Selective removal of certain elements in a multicomponent material structure, via thermal decomposition or chemical etching, also leads to the formation of porous

*Disclaimer: Official contribution of the National Institute of Standards and Technology; not subject to copyright in the United States.

architectures within the solid material (Mansoori et al., 2007; Rouquerol et al., 1994a). Figure 3 shows the scanning electron microscopy (SEM) image of hollow silica spheres prepared through chemical dissolution of the polystyrene nanoparticles used as template (Mansoori et al., 2007). The natural deposition of sediments in geologically ancient seas also yields porous rocks and formations, which are composed of multiple minerals and contain intracrystalline and interparticle voids (Dandekar, 2006). Porosity in rocks can also be induced by natural geological processes following deposition, such as weathering or dissolution, dolomitization (a cation exchange reaction that increases porosity), and formation of fractures (Dandekar, 2006; Tiab and Donaldson, 2012). Figure 4 presents an example of the types of porosity found in sandstone formations (Tiab and Donaldson 2012).

The most common characteristics of porous solids are specific surface area (SSA), average pore size, and pore-size distribution (Rouquerol et al., 1994a). Knowledge of such material characteristics is critical for ensuring material quality requirements and designing new porous materials for various industrial applications. SSA is defined as the area of solid surface per unit mass of material. The surface area detectable by a particular technique depends on the size of the "yardstick" or probe used in the measurement (e.g., gas molecule of a given size and light of a certain wavelength), experimental conditions, and pore or surface model employed in the calculations (Klobes et al., 2006; Rouquerol, 1994a). Therefore, the recorded values depend on both the instrument and assumptions employed. Complexities also exist for pore-size measurements, particularly given the large variability and irregularity in pore shapes. As shown in Figure 5, pores can have different shapes and accessibility to gases or liquids: (a) closed pores isolated from other pores, (b) ink-bottle-shaped pores that are closed only at one end, (c) cylindrical pores that are open at both ends, (d) funnel-shaped open pores, (e) cylindrical open interconnected pores, and (f) cylindrical pores that are open only at one end (Klobes et al., 2006; Rouquerol, 1994a). The sequence in which pores sizes are measured (or detected) depends on the physical principle or detection method, which is highly affected by variations in pore shapes and interconnectivity between pores. In the International Union of Pure and Applied Chemistry (IUPAC) the system for classifying porous materials, pore sizes are grouped as follows: micropores (widths < 2 nm), mesopores ($2\text{ nm} < \text{widths} < 50$ nm), and macropores (widths > 50 nm) (Klobes et al., 2006; Rouquerol, 1994a, 1999).

TECHNIQUES

The large variety of porous structures and industrial applications has led to the development and use of many experimental techniques for determining the various characteristics of porous solids (Rouquerol et al., 1994a). Gas sorption (Rouquerol et al., 1999; Lowell et al., 2006; Keller and Staudt, 2005; Asthana et al., 2006), liquid intrusion (Rouquerol et al., 1999; Lowell

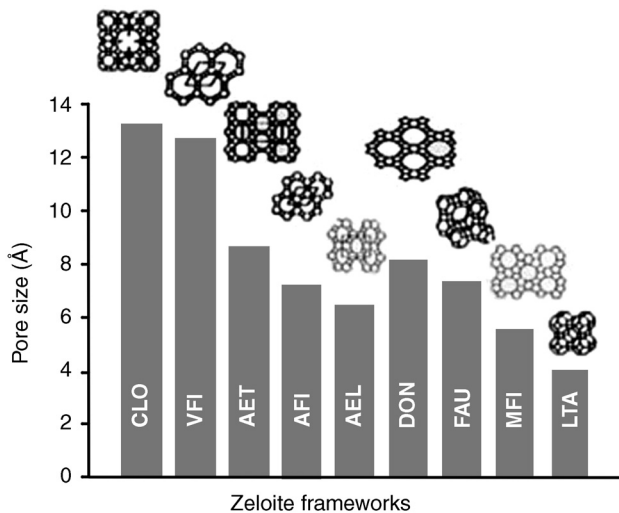


Figure 1. Pore sizes of different zeolites ($1 \text{ nm} = 10 \text{ \AA}$). The three-letter acronyms shown represent the crystal structure of the zeolite displayed at the top of each column. Reprinted with permission from Auerbach et al. (2003).

et al., 2006; Ramachandran and Beaudoin, 2001; Sibilia, 1996, microscopy (Khayet and Matsuura, 2011; Reese, 2006), and x-ray and neutron scattering (Aligizaki, 2006; Feigin and Svergun, 1987; Silverstein et al., 2011; Wong, 1999) are the most common methods for porosity characterization, although other techniques such as thermoporometry (Rodriguez-Reinoso et al., 1991; Somasundaran, 2006; Brown and Gallagher, 2003), inverse size exclusion chromatography (Rouquerol, 1994b; Unger et al., 2011; Striegel et al., 2009), positron annihilation spectroscopy (Petkov et al., 2003), nuclear magnetic resonance (Wong, 1999; Konsta-Gdoutos, 2006; Staf and Han, 2006), muon spin resonance (Lee et al., 1999), and ultrasonic attenuation methods (Thompson and Chimenti, 1993; Kutz, 2002) can also provide an independent assessment of porosity. As shown in Figure 6, each method provides reliable information for different pore-size ranges based on the specifics of the measuring physical principle. The preference for using one method over another depends on the expected range of pore sizes,

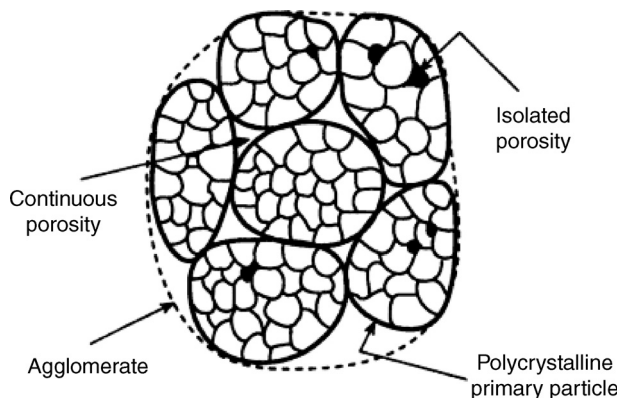


Figure 2. Schematic diagram of agglomerate consisting of dense and polycrystalline particles. Reprinted with permission from Rahaman (2003).

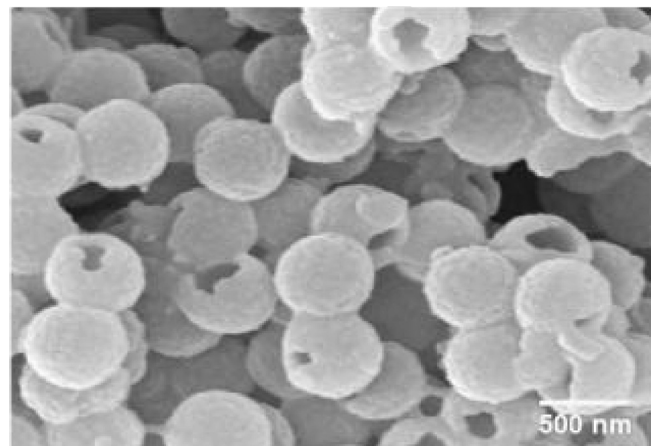


Figure 3. Scanning electron microscopy (SEM) image of hollow silica spheres prepared by using polystyrene nanoparticles as a template. Polystyrene nanoparticles are removed via dissolution in toluene. Reprinted with kind permission from Springer Science + Business Media: (Mansoori et al., 2007).

material properties, instrument availability, sample geometry requirements, and final application. For example, gas separation sorbent materials (usually powders) are typically characterized using gas sorption methods (Keller and Staudt, 2005) while membranes via microscopy (Li et al., 2008) and fluid flow (Khayet and Matsuura, 2011). If resources are available, more than one method can be used for cross verification though there will be differences inherently associated with the use of different detection methods. For materials containing hierarchical pore structures that span multiple length scales from angstroms to millimeters, several instruments may be needed to provide adequate characterization. In this article, we provide a brief description of the most common porosity measurement methods.

Gas Sorption

The physical adsorption of gases by porous materials at subcritical temperatures, which involves weak intermolecular forces, has been widely used for micropore and mesopore analysis (Rouquerol et al., 1999; Lowell et al., 2006; Keller and Staudt, 2005). Prior to gas

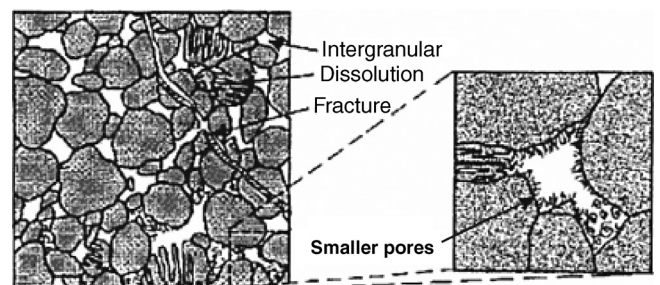


Figure 4. Types of porosity found in geological sandstone reservoirs. Reprinted from Tiab and Donaldson (2012), Copyright 2012, with permission from Elsevier.

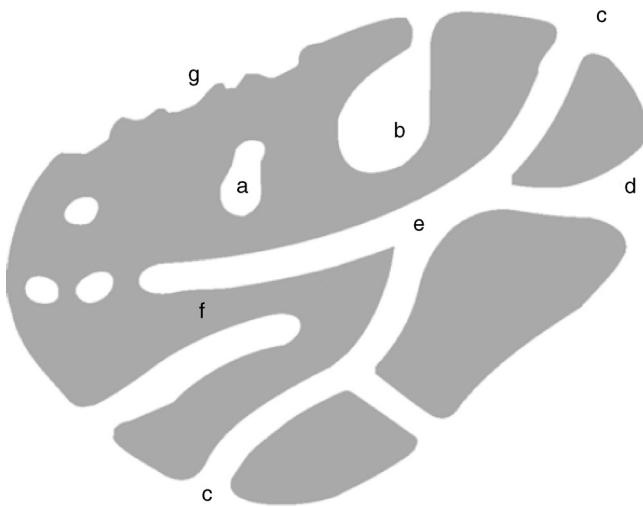


Figure 5. Schematic cross-section of a porous solid (Klobes et al., 2006).

adsorption experiments, the sample must be evacuated or degassed to remove moisture, vapor, and any other unwanted gas species from the pore surface. Sample evacuation can be achieved via heating under vacuum or flushing with an inert gas. In order to avoid exceeding sample degradation temperatures during degassing, the thermal stability of the sample must be known. In the case of samples sensitive to heating, water removal can be accomplished in a dessicator (Lowell et al., 2006). The evacuated sample of known mass is transferred to the sorption chamber, typically using a glove box to avoid the exposure of the sample to air after degassing. While inside the sorption chamber, the sample is progressively dosed with the known amounts of gas admitted into the sorption chamber in incremental pressure steps, allowing sufficient time to reach equilibrium at every step (Rouquerol et al., 1999). Once the final target adsorption

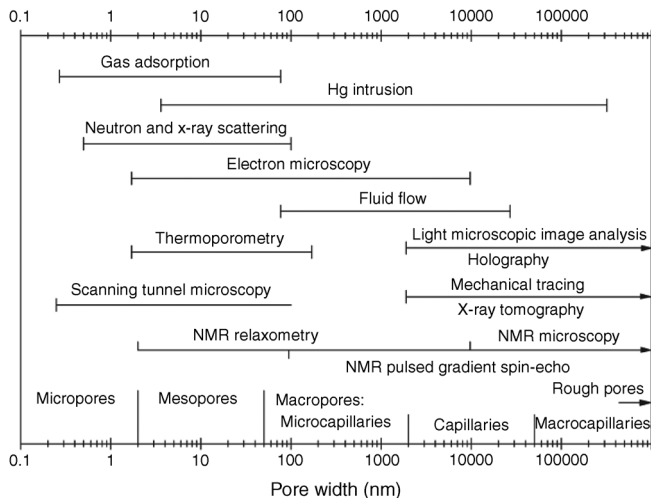


Figure 6. Pore-size measurement range for different methods (Klobes et al., 2006).

pressure step is achieved, usually saturation pressure (p_0), the reverse process takes place (desorption) in which gas is progressively withdrawn until the initial state is reached. The quantity of gas adsorbed (normalized by sample mass) at every step during the adsorption and desorption process is recorded as a function of the relative pressure (p/p_0) of the adsorptive gas and the resulting adsorption–desorption curve is known as a gas sorption isotherm. Some gas–adsorbent systems exhibit hysteretic sorption behavior in which the desorption branch of the isotherm follows a different path than the adsorption (Lowell et al., 2006). Based on sorption data, pore models, and other assumptions, the surface area and pore-size distribution can be estimated (Rouquerol et al., 1994a). Although a priori sample evacuation is required, the great advantage of the gas sorption technique lies on its nondestructive nature (Lowell et al., 2006). An example of sorption isotherms for calcined mesoporous silica is shown in Figure 7a (Mal et al., 2002).

For the measurement of the quantity of gas adsorbed at every pressure point, there are volumetric and gravimetric techniques. Volumetric methods are generally employed for nitrogen at 77 K and argon at 87 K. Gravimetric techniques are more common for studying the adsorption of vapors at temperatures near ambient conditions (Klobes et al., 2006). The pore-size distribution measurements are typically carried out using the adsorption branch of the isotherm although the desorption branch can also be used (Lowell et al., 2006). The pore-size range that can be measured with gas sorption measurements depends on the size of the gas molecule employed as the probe and the capability of the equipment to achieve high relative pressures. In the case of nitrogen, the smallest detectable pore size is about 0.4 nm and the largest is approximately 300 nm (Klobes et al., 2006). However, for comparing pore-size distributions of materials containing micropores (pore sizes < 2 nm), adsorptive molecules smaller than nitrogen (e.g., argon) could provide more reliable data (Lowell et al., 2006). An example of pore-size distribution for mesoporous silica is shown in Figure 7b (Mal et al., 2002).

The determination of pore-size distribution in mesoporous materials requires the use of methods based on the following Kelvin equation (Klobes et al., 2006; Lowell et al., 2006):

$$r_k = \frac{2 \cdot V_m \cdot \gamma \cdot \cos \theta}{R \cdot T \cdot \ln\left(\frac{p}{p_0}\right)} \quad (2)$$

where r_k is the radius of curvature of the condensed gas inside the pore, γ is the surface tension, V_m represents the molar gas volume of an ideal gas, and θ the contact angle.

For the calculation of the pore size, the value of r_k is corrected according to the assumed pore geometry (e.g., cylindrical or slit-shaped pore) and thickness of the layer of gas adsorbed on the pore surface. For example, in

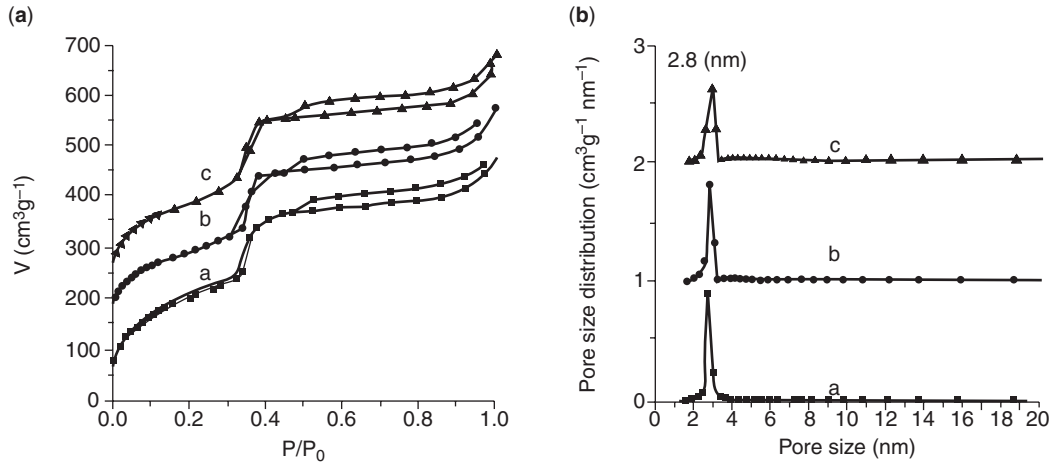


Figure 7. Nitrogen sorption isotherms (a) and pore-size distribution curves (b) of three different calcined mesoporous silica samples. Reprinted from (Mal et al., 2002), Copyright 2002, with permission from Elsevier.

the case of a cylindrical pore, the radius (r_p) is corrected by adding the thickness ($r_p = r_k + t$), whereas in the case of a slit-shaped pore, the slit-width (d_p) is given by $d_p = r_k + 2t$. Several methods exist for estimating the thickness (Klobes et al., 2006).

Due to the characteristic molecular dimensions of micropores, which enhance interactions between gas molecules and pore surface, separate models and methods of data analysis have been developed for micropore analysis (Klobes et al., 2006; Rouquerol et al., 1999; Lowell et al., 2006) including Dubinin–Radushkevitch, Horvath–Kawazoe, *t*-plot method, and others. In addition, employing a range of gas molecules of different sizes can provide a more realistic picture of the pore microstructure (Lowell et al., 2006).

The Brunauer–Emmett–Teller (BET) method has been applied for several decades to physisorption isotherm data to yield the values of the surface area. The first step in calculating the BET surface area involves the calculation of the monolayer capacity according the following equation:

$$\frac{p}{n^a(p_0-p)} = \frac{1}{n_m^a C} + \frac{(C-1)}{n_m^a C} \cdot \frac{p}{p_0} \quad (3)$$

where n^a is the amount adsorbed at the relative pressure p/p_0 , n_m^a represents the monolayer capacity, and C is a constant (Klobes et al., 2006; Rouquerol et al., 1994a).

The linear curve obtained from plotting $\frac{p}{n^a(p_0-p)}$ versus $\frac{p}{p_0}$, at relative pressures between 0.05 and 0.3, is used to calculate the value of the monolayer capacity, n_m^a . Based on the n_m^a obtained and the average molecular cross-sectional area (a_m) assumed for the adsorptive molecule, the BET surface area can be estimated according to the following equation:

$$SA_{\text{BET}} = n_m^a \cdot L \cdot a_m \quad (4)$$

where L is the Avogadro constant (Klobes et al., 2006). A common assumption for nitrogen is that the BET

monolayer is close-packed (Klobes et al., 2006), which yields a value of a_m of 0.162 nm^2 (at 77 K). The value of the surface area obtained excludes the contribution from those pores smaller than the gas molecules used as probe.

Fully automated commercial instruments are commonly used for gas sorption measurements except in laboratories where custom units have been developed to enhance certain measurement features required to meet specific research needs. Because porosity data depend on both the experimental technique used and the theoretical method employed for data analysis, certified reference materials and standardized measurement procedures are used to calibrate and check the performance of the sorption equipment. Certified reference materials for the surface area and pore size are obtainable from the following internationally recognized standard organizations: Bundesanstalt für Materialforschung und -prüfung (BAM, Germany), Institute for Reference Materials and Measurements (IRRM, European Community), National Institute of Standards and Technology, (NIST, USA), and LGC Standards (LGC, UK). Standardized measurement procedures are available from international organizations such as the International Organization for Standardization (ISO, Geneva) and the American Society for Testing Materials (ASTM International).

Liquid Intrusion

Liquid intrusion by a nonwetting liquid is a very widely accepted method for analyzing meso and macropore scales (Rouquerol et al., 1994a), particularly between 4 nm and 60 μm . The most commonly used method is known as mercury porosimetry. In cases where a sample is known to react with mercury (e.g., zinc and gold), careful passivation of the sample or the use of an alternative nonwetting fluid must be considered. The experimental procedure in mercury porosimetry is similar to gas sorption. In a typical experiment, a sample of known mass is placed inside a sealed enclosure

(penetrometer) and evacuated to remove unwanted species from the pore space (e.g., vapor, moisture, and air) via heating under vacuum or flushing with an inert gas. For heat-sensitive samples, prior drying in a dessicator might be required (Lowell et al., 2006). After evacuation, the nonwetting fluid is progressively introduced into the chamber through incremental hydraulic pressure steps. The volume of mercury is recorded as a function of applied pressure (Klobes et al., 2006).

Based on the external pressure p (MPa) required to push the mercury into a cylindrical pore of radius r_p (μm), pore sizes can be obtained according to the following Washburn equation (Klobes et al., 2006):

$$r_p = \frac{2 \cdot \gamma \cdot \cos \theta}{p} \quad (5)$$

where γ represents the surface tension of the liquid (N/m) and θ the contact angle. For liquid mercury, the surface tension at room temperature is approximately 0.480 N/m and the contact angle is typically assumed to be 140° (Klobes et al., 2006). A mercury porosimeter can measure pore sizes from as low as 1.8 nm to as high as $200 \mu\text{m}$ (Lowell et al., 2006), depending on the specific pressure capabilities of the equipment and the contact angle assumed in the calculations. The lowest filling pressure achievable by the instrument will determine the largest pore size and the highest pressure will establish the smallest pore size. Note that the radius r_p represents the size of an equivalent cylindrical pore that requires a given pressure to be filled. Therefore, the validity of pore-size measurements via mercury porosimetry also depends on the pore geometry assumed.

A plot of the intruded (and extruded) volume of mercury (V) as a function of applied pressure (p) is known as a porosimetry curve. Based on the function $V = V(p)$, the total surface area can be estimated according to the following equation (Klobes et al., 2006):

$$SA_{\text{Hg_method}} = \frac{1}{\gamma \cos \theta} \int_{V_{\text{Hg},0}}^{V_{\text{Hg},\text{max}}} p \cdot dV \quad (6)$$

The values of surface area obtained from mercury porosimetry exclude contributions from very small pores. Therefore, a complete agreement with the gas-sorption-based surface area measurements should not be expected. As in the case of gas sorption equipment, commercial mercury porosimetry instruments are readily available. Also, certified reference materials and standard measurement protocols for mercury porosimetry are accessible from the international standard organizations mentioned earlier to enable equipment calibration and allow data comparisons across laboratories worldwide.

Figure 8 displays an example of mercury porosimetry data for a porous glass showing the volume of mercury intruding into the pore space available as applied pressure increases from point A to B. Upon depressurization (from point B to C), the extrusion curve does not follow the same path, compared to intrusion, indicating some mercury is permanently retained in the pores (Klobes

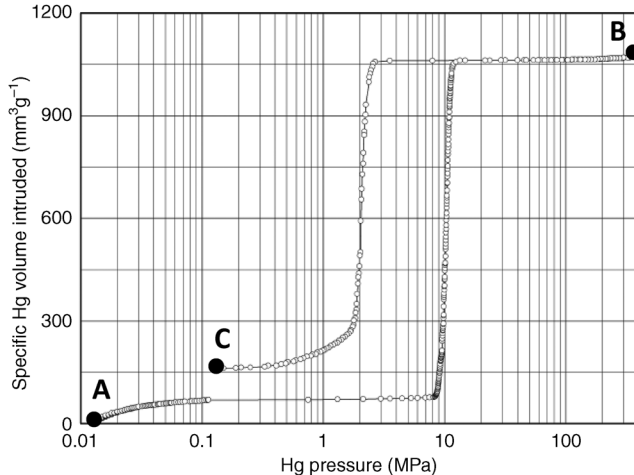


Figure 8. Intrusion-extrusion curve (volume versus pressure curve) of a porous glass (Klobes et al., 2006).

et al., 2006). The permanent entrapment of mercury upon extrusion makes this technique destructive. Another disadvantage of this method involves the use of mercury, which should be handled with the same care as other chemicals in the laboratory (Lowell et al., 2006). Local safety regulations should be checked for guidelines on the proper use, handling, and disposal of mercury. Permissible exposure limits for mercury can be found in reference U.S. Department of Labor Occupational Safety & Health Administration, OSHA.

Microscopy

Microscopy allows the reliable analysis of the pore geometry and sizes in the mesopore range or above via direct observations of thin cross-sections of solid materials. Depending on the specific pore-size resolution required, optical or electron microscopy can be used. Detailed equipment information can be found in Chapters ELECTRON TECHNIQUES and OPTICAL IMAGING AND SPECTROSCOPY. Due to the wavelength of light available in optical microscopy, its lateral resolution is in the order of 200 nm (Reese, 2006). Smaller features are typically analyzed by electron and atomic force microscopy techniques. Sample preparation is an important consideration when analyzing samples via microscopy. For large samples such as rocks and cement components, the use of thin sections is a very common practice. Although powder samples are also suitable for analysis, the use of thin sections allows for analysis of all sample components at the same level or depth. A variety of techniques can be employed for improving contrast between matrix and pores (Müller-Reichert, 2010; Hayat, 2000), for example: surface replication, shadowing, or impregnation of the pore space with fluorescent resin. Nonconducting samples, such as polymeric membranes, require a thin metallic coating to avoid electrostatic charging during electron microscopy analysis (Reese, 2006). The collection of a statistically large number of samples and measurements is necessary for a comprehensive characterization of the pore geometry

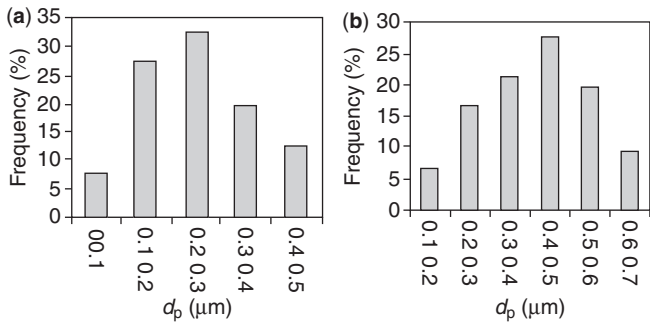


Figure 9. Pore-size distribution obtained by software analysis of field emission scanning electron micrographs of two commercial membranes: (a) membrane A and (b) membrane B. The total number of pores per image used in the calculations ranged from 900 to 1300. Reprinted from Khayet and Matsuura (2011), Copyright 2011, with permission from Elsevier.

and size distribution. Numerous techniques and commercial software (Khayet and Matsuura, 2011; Bennett et al., 1991) are readily available for the automatic processing of 2D images of porous materials to yield the ratio of the fractional areas of pore space to solid matrix, pore-size distribution, distribution of pore lengths and widths, and specific surface area. Figure 9 presents the pore-size distribution of two commercial distillation membranes (Khayet and Matsuura, 2011), both based on image analyses.

Image analysis via microscopy provides a direct measurement where no models or further assumptions are required. However, the requirement for having either a plane cross-sectional sample or application of a metal coating makes microscopy-based techniques destructive. In addition, the suitability of microscopy for a particular sample depends on the effect of sample preparation requirements (e.g., thin sectioning, contrast enhancement method used, and metal coating procedure applied) on its pore structure. Another important aspect relates to potential underestimation of the specific surface area if the instrument employed cannot resolve the smallest pore features in the sample (Rouquerol et al., 1994a). Thin section samples are commonly used in the petroleum industry to analyze the pore structure of rocks and geological formations. However, additional measurements may be needed to complete the material's evaluation. In the case of rock samples, fluid flow measurements are needed for predicting many of the important properties for the proper assessment of porous media in the oil industry, for example, permeability (Civan, 2000). Examples of carbonate and sandstone thin sections are shown in Figure 10 (Tsakiroglou et al., 2009).

Light, X-ray, and Neutron Scattering

Light, x-ray, and neutron scattering can be used for porosity characterization as solid material and void spaces have different refractive indices (light sensitive) (Wong, 1999), electronic structure or density (x-ray sensitive) (Glatter and Kratky, 1982), and nuclear structure or neutron scattering length density (neutron sensitive)

(Elias, 2008). In brief, the pore-size distribution and surface area can be deduced from measurements of the angular distribution of scattered intensities. The techniques are known as light scattering (static and dynamic), small angle x-ray scattering (SAXS), and small angle neutron scattering (SANS). For detailed information on these methods, see article on DYNAMIC LIGHT SCATTERING within the chapter on OPTICAL IMAGING AND SPECTROSCOPY, and also see Chapters NEUTRON TECHNIQUES and X-RAY TECHNIQUES.

In contrast to gas sorption techniques, scattering techniques require no pretreatment of samples prior to data collection and thus can be analyzed in the presence of a gas or air (Rouquerol et al., 1994a). However, material properties such as chemical composition and opacity must be considered for selecting the scattering method to be used (Wong, 1999). For example, opaque materials are not well suited for light scattering but are not a problem for SAXS or SANS. In addition, the material used as sample container must be transparent to the incident beam. Accordingly, the samples are placed in enclosures made of window materials suitable for every technique, for example, mica or thin polymeric film for SAXS (Aligizaki, 2006), and quartz for SANS (Rouquerol et al., 1994a). While dry powder samples can simply be placed in between thin polymer films (Rouquerol et al., 1994a), liquid-containing samples may require the use of a special sample holder to keep the liquid in place. The characterization of porous materials containing high Z-elements using SAXS requires sample thicknesses in the order of 0.25 mm (Aligizaki, 2006) while the desired path length for SANS is typically between 1 and 5 mm (Rouquerol et al., 1994a; Aligizaki, 2006). Compared to SANS, x-ray-based scattering provides higher sensitivity to samples containing heavy elements. Neutron-based scattering is ideal for materials containing light elements such as hydrogenous compounds. For absolute intensity measurements, the powder sample density and thickness must be recorded.

Both SAXS and SANS experiments require special facilities with a source of radiation, a monochromator, collimation system, sample holder, and a detector. For equipment details see chapters on NEUTRON TECHNIQUES and X-RAY TECHNIQUES. In a typical scattering experiment, the sample is bombarded with a monochromatic beam of light, x-rays, or neutrons, of wavelength λ_o and intensity I_o , which interacts with the sample components, including void spaces and solid matrix (Aligizaki, 2006). Such interaction produces a range of scattering intensities, which are measured as a function of the scattering angle ($2\theta_s$) between the incident and scattered beams, as defined by $d \sim \lambda / 2\theta_s$ where d is the size of the feature (e.g., pore diameter) and λ the wavelength of radiation (e.g., light, x-rays, or neutrons) (Rouquerol et al., 1994a). A scattering curve can then be obtained by plotting the scattering intensity, $I(Q)$ as a function of the scattering angle $2\theta_s$ or scattering vector Q , (for a detailed definition of Q , see article SMALL ANGLE NEUTRON SCATTERING). Pore structure information is derived from analyses of small angle scattering data through the fitting of scattering data to models

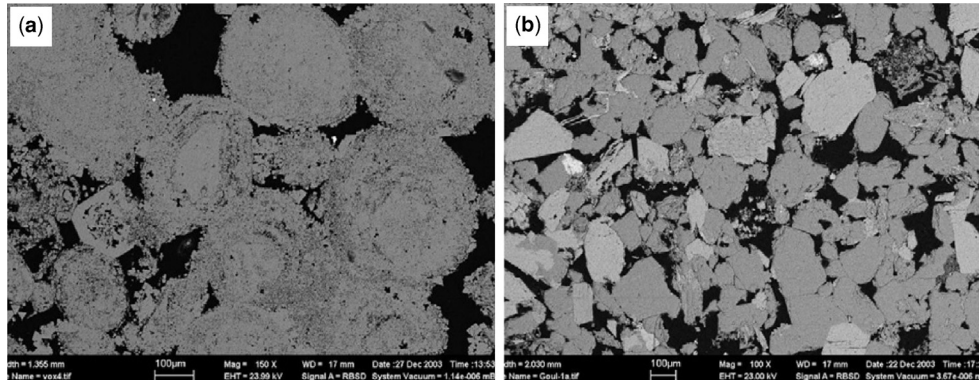


Figure 10. Backscattered electron microscope images of thin section samples of: (a) carbonate and (b) sandstone. Black areas in the image represent pore spaces between grains. Reprinted from Tsakiroglou et al. (2009), Copyright 2009, with permission from Elsevier.

(Aligizaki, 2006) and the use of standard plots, numerical methods, and approximations (e.g., Guinier, Porod, and Zimm) (Glatter and Kratky, 1982) to extract characteristic slopes and intercepts. The interpretation of scattering data requires prior knowledge of the expected morphological features in the sample in order to assume a suitable pore network geometry and reduce the number of unknowns (Aligizaki, 2006). Methods for data analysis provide the size of various regions with different relative densities via fitting to chosen models. While x-ray and neutron scattering are techniques sensitive to the relative variation of the sample composition, these measurements do not provide absolute densities. Therefore, results derived from these techniques should be treated with caution and be complemented with data from other methods such as microscopy and gas sorption. Figure 11 presents data for two mesoporous silica samples containing pores of different geometry and size,

with diameters of approximately 2 nm (cylindrical) and 13 nm (spherical) (Smarsly et al., 2005).

Scattering techniques can be used to measure the surface area between the hollow and solid structure as well as the void-to-solid matrix volume fractions attributed to the presence of intraparticle pores, particle sizes, and interparticle spaces. The type of radiation in each technique determines the spatial resolution, which ranges from 5 to 50 nm for SAXS, from 50 to 500 nm for SANS, and from 200 to 20,000 nm for light scattering. Scattering techniques cover mean pore sizes between 1 and 1000 nm (Rouquerol et al., 1994a). The value of the surface area obtained from scattering data excludes contributions outside the detectable pore-size range. Thus, complete agreement with gas sorption-based surface area measurements should not be expected. For highly crystalline materials, information on pore widths in the micropore range can be obtained from

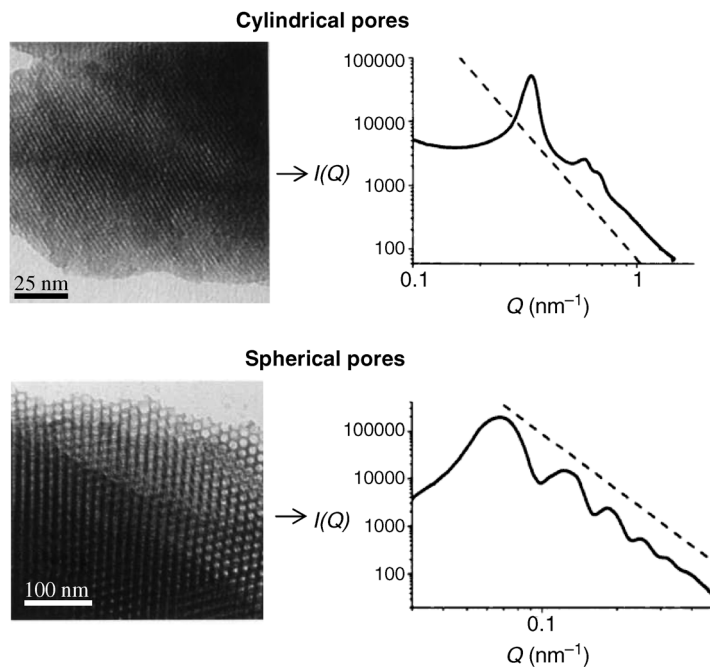


Figure 11. Transmission electron microscopy images (Left) and SAXS curves (Right) of two mesoporous silica samples containing different pore geometries: cylindrical (Top) and spherical (Bottom). The Porod asymptote is indicated by the dashed line in both cases. Reprinted with kind permission from Springer Science + Business Media: (Smarsly et al., 2005).

x-ray and neutron diffraction data (Ikeda et al., 2010; McCusker, 2004; Wessels et al., 1999; Wright, 2008; Cheetham et al., 1986; Newsam, 1991).

Scattering techniques have the great advantage of being nondestructive and have particularly great sensitivity to the presence of closed pores (Rouquerol et al., 1994a; Wong, 1999), which are undetectable by gas sorption measurements as gas molecules cannot access closed pores. In cases where the material is suspected to have closed porosity, index-match light scattering (Wong, 1999) or contrast-match SANS (Reese, 2006; Aligizaki, 2006) experiments can be performed in which the sample is analyzed before and after impregnation with a liquid of similar scattering properties to the solid matrix. A material containing closed porosity will continue to show the presence of certain pores (closed pores) after impregnation.

SUMMARY

Due to the inherent difference in the physical principles for each method, perfect agreement between the values of total porosity, surface area, average pore size, and distribution obtained for all techniques is not possible. Similarly, a perfect agreement between two techniques will not necessarily validate the values obtained. Within a given technique, the postsynthesis history of the sample should be taken into account as many material applications require postsynthesis treatments (e.g., annealing and mechanical forming), which can lead to different porosity. All techniques have advantages and disadvantages, in particular with respect to the assumptions made to derive the results. An approach to understand how these techniques differ from each other could involve the evaluation of a reference model porous material using the techniques under consideration. The selection criteria should extend beyond the expected pore-size range and take into account the suitability of sample preparation, material property, and sample geometry requirements for every technique as well as the intended material's application.

LITERATURE CITED

- Aligizaki, K. K. 2006. Pore Structure of Cement-Based Materials: Testing, Interpretation, and Requirements. (Taylor & Francis, New York).
- Asthana, R., Kumar, A., and Dahotre, N. 2006. Materials Science in Manufacturing. (Academic Press, Burlington).
- Auerbach, S. M., Carrado, K. A., and Dutta, P. K. 2003. Handbook of Zeolite Science and Technology. (Marcel Dekker Inc., New York).
- Bennett, R. H., Bryant, W. R., and Hulbert, M. H. 1991. Microstructure of Fine-Grained Sediments: From Mud to Shale. (Springer-Verlag, New York).
- Cheetham, A. K. et al. 1986. Crystal structure determination by powder neutron diffraction at the spallation neutron source, ISIS. *Nature* 320:46–48.
- Civan, F. 2000. Reservoir Formation Damage: Fundamentals, Modeling, Assessment, and Mitigation. (Gulf Publishing Company, Houston).
- Dandekar, A. Y. 2006. Petroleum Reservoir Rock and Fluid Properties. (CRC Press/Taylor & Francis Group, LLC, Boca Raton, FL).
- Deng, H. et al. 2005. Monodisperse magnetic single-crystal ferrite microspheres. *Angewandte Chemie International Edition* 44:2782–2785.
- Elias, H.-G. 2008. Macromolecules: Physical Structures and Properties. Vol. 3 (Wiley-VCH, Weinheim).
- Feigin, L. A. and Svergun, D. I. 1987. Structure Analysis by Small-Angle X-Ray and Neutron Scattering. (Plenum Press, New York).
- Brown, M. E. and Gallagher, P. K. 2003. Handbook of Thermal Analysis and Calorimetry: Applications to Inorganic and Miscellaneous Materials. Vol. 2 (Elsevier B.V., Amsterdam).
- Glatter, O. and Kratky, O. 1982. Small Angle X-ray Scattering. (Academic Press, London).
- Hayat, M. A. 2000. Principles and Techniques of Electron Microscopy: Biological Applications. Fourth edn, (Cambridge University Press, Cambridge).
- Ikeda, T., Kayamori, S., Oumi, Y., and Mizukami, F. 2010. Structure analysis of Si-atom pillared lamellar silicates having micropore structure by powder x-ray diffraction. *The Journal of Physical Chemistry C* 114:3466–3476.
- Keller, J. and Staudt, R. 2005. Gas Adsorption Equilibria: Experimental Methods and Adsorptive Isotherms. (Springer Science + Business Media, Boston).
- Khayet, M. and Matsuura, T. 2011. Membrane Distillation: Principles and Applications. (Elsevier B.V., Amsterdam).
- Klobes, P., Meyer, K., and Munro, R. G. 2006. Porosity and specific surface area measurements for solid materials. *NIST Recommended Practice Guide*.
- Konsta-Gdoutos, M. S. 2006. Measuring, Monitoring, and Modeling Concrete Properties. (Springer, Dordrecht, the Netherlands).
- Kutz, M. 2002. Handbook of Materials Selection. (John Wiley & Sons, New York).
- Lee, S. L., Kilcoyne, S. H., and Cywinski, R. 1999. Muon Science: Muons in Physics, Chemistry and Materials. (Taylor & Francis Group, New York).
- Li, N. N., Fane, A. G., Ho, W. S. W., and Matsuura, T. 2008. Advanced Membrane Technology and Applications. (John Wiley & Sons, Hoboken, NJ).
- Lowell, S., Shields, J. E., Thomas, M. A., and Thommes, M. 2006. Characterization of Porous Solids and Powders: Surface Area, Pore Size and Density (Springer, Dordrecht, the Netherlands).
- Mal, N. K., Kumar, P., and Fujiwara, M. 2002. Sorption properties and hydrothermal stability of MCM-41 prepared by pH adjustment and salt addition. *Studies in Surface Science and Catalysis* 141:445–452.
- Mansoori, G. A., George, T. F., Assoufid, L., and Zhang, G. 2007. Molecular Building Blocks for Nanotechnology: From Diamondoids to Nanoscale Materials and Applications. (Springer, New York).
- McCusker, L. B. 2004. The Art of Zeolite Structure Analysis. *Studies in Surface Science and Catalysis*, 154:41–51.
- Müller-Reichert, T. 2010. Electron Microscopy of Model Systems. (Academic Press, Burlington).
- Newsam, J. M. 1991. Developments in x-ray and neutron diffraction methods for zeolites Vol. 60 In Chemistry of Microporous Crystals (T. Inui, S. Namba, T. Tatsumi, eds.), pp. 133–140 (Elsevier Science Publisher B.V., Amsterdam).

- U.S. Department of Labor Occupational Safety & Health Administration (OSHA), Safety and Health Topics. Available at <http://www.osha.gov/SLTC/>
- Petkov, M. P., Wang, C. L., Weber, M. H., Lynn, K. G., and Rodbell, K. P. 2003. Positron annihilation techniques suited for porosity characterization of thin films. *The Journal of Physical Chemistry B* 107:2725–2734.
- Rahaman, M. N. 2003. Ceramic Processing and Sintering. Second edn, (Marcel Dekker Inc., New York).
- Ramachandran, V. S. and Beaudoin, J. J. 2001. Handbook of Analytical Techniques in Concrete Science and Technology: Principles, Techniques, and Applications. (William Andrew Publishing, LLC/Noyes Publications, Norwich).
- Reese, J. P. 2006. New Nanotechnology Research. (Nova Science Publishers, Inc.).
- Rodriguez-Reinoso, F., Rouquerol, J., Sing, K. S. W., and Unger, K. K. 1991. Characterization of Porous Solids II. (Elsevier, Amsterdam).
- Rouquerol, F., Rouquerol, J., and Sing, K. 1999. Adsorption by Powders and Porous Solids: Principles, Methodology and Applications. (Academic Press, London).
- Rouquerol, J. et al. 1994a. Recommendations for the characterization of porous solids. *Pure & Applied Chemistry* 66:1739–1758.
- Rouquerol, J., Rodriguez-Reinoso, F., Sing, K. S. W., and Unger, K. K. 1994b. Characterization of Porous Solids III. (Elsevier Science B.V., Amsterdam).
- Sibilia, J. P. 1996. A Guide to Materials Characterization and Chemical Analysis. Second edn, (Wiley-VCH, Inc., New York).
- Silverstein, M. S., Cameron, N. R., and Hillmyer, M. A. 2011. Porous Polymers. (John Wiley & Sons, Inc., Hoboken, NJ).
- Smarsly, B., Groenewolt, M., and Antonietti, M. 2005. SAXS analysis of mesoporous model materials: Validation of data evaluation techniques to characterize pore size, shape, surface area, and curvature of the interface. *Progress in Colloid and Polymer Science* 130:105–113.
- Somasundaran, P. 2006. Encyclopedia of Surface and Colloid Science Vol. 6 (Taylor & Francis, Boca Raton, FL).
- Stapf, S., and Han, S.-I. 2006. NMR Imaging in Chemical Engineering. (Wiley-VCH Verlag GmbH & Co. KGaA, Weinheim).
- Striegel, A. M., Yau, W. W., Kirkland, J. J., and Bly, D. D. 2009. Modern Size-Exclusion Liquid Chromatography: Practice of Gel Permeation and Gel Filtration Chromatography. Second edn, (John Wiley & Sons, Inc., Hoboken, NJ).
- Thompson, D. O. and Chimenti, D. E. 1993. Review of Progress in Quantitative Nondestructive Evaluation. (Plenum Press, New York).
- Tiab, D. and Donaldson, E. C. 2012. Petrophysics: Theory and Practice of Measuring Reservoir Rock and Fluid Transport Properties. Third edn, (Gulf Professional Publishing, Waltham).
- Tsakiroglou, C. D., Ioannidis, M. A., Amirtharaj, E., and Vizika, O. 2009. A New Approach for the Characterization of the Pore Structure of Dual Porosity Rocks. *Chemical Engineering Science* 64:847–859.
- Unger, K. K., Tanaka, N., and Machtejevas, E. 2011. Monolithic Silicas in Separation Science: Concepts, Syntheses, Characterization, Modeling and Applications. (Wiley-VCH, Weinheim).
- Warren, S. C. et al. 2008. Ordered mesoporous materials from metal nanoparticle-block copolymer self-assembly. *Science* 320:1748–1752.
- Wessels, T., Baerlocher, C., and McCusker, L. B. 1999. Single-crystal-like diffraction data from polycrystalline materials. *Science* 284:477–479.
- Wong, P.-z. 1999. Methods in the Physics of Porous Media. Vol. 35 (Academic Press, San Diego).
- Wright, P. A. 2008. Microporous Framework Solids. (The Royal Society of Chemistry, Cambridge).

KEY REFERENCES

- Lowell, et al., 2006. See above.
Provides an overview of principles associated with the characterization of solids with regard to their surface area, pore size and density based on gas adsorption and mercury porosimetry.
- Hayat, 2000. See above.
Describes fundamental principles and techniques of electron microscopy for materials with biological applications.
- Rouquerol, et al., 1999. See above.
Reviews theoretical and practical aspects of adsorption by powders and porous solids and presents some of the adsorptive properties of common materials such as activated carbons, oxides, clays and zeolites.
- Wong, P.-z. 1999. See above.
Presents several techniques for characterizing porous media, in particular scattering methods, from the standpoint of an experimental physicist.